CANADIAN JOURNAL OF EXPLORATION GEOPHYSICS
VOL. 24, NO. 2 (DECEMBER 1988), P. 101-109

A PRACTICAL APPROACH TO PARAMETER SELECTION FOR MODELLING WITH THE REFLECTIVITY METHOD

Z. HAJNAL[1], B.I. PANDIT[1] AND M.R. STAUFFER[1]

ABSTRACT

A practical and simple method is developed for the selection of computational parameters to be used when the reflectivity method is applied to generate synthetic seismograms for a horizontally layered Earth. The actual sedimentary-strata-based design of parameters, which are easily computed, eliminates the numerical noise that generally contaminates seismic records produced by using the standard trial-error procedures to define the best parameters. In the selection process, special attention is given here to the typical hydrocarbon exploration environment.

The computations automatically provide all *P*-wave arrivals, including multiples, in a single calculation, for any number of traces and offsets. Examples illustrate the types of numerical artifacts created by poor parameter or kernal-function selection.

The derived seismograms are clean and are computed without costly experimental computer runs. The control of numerical artifacts permits acquisition of theoretical responses from models with intricate acoustic characteristics.

INTRODUCTION

The reflectivity method (Fuchs, 1968; Fuchs and Müller, 1971) is a powerful technique for computing synthetic seismograms and for modelling some intricate response characteristics of the Earth. In recognition of the exceptional power of the method it has had many improvements and extensions (Kennett, 1974, 1979, 1980, 1983; Kind, 1978, 1979; Fryer, 1980; Mallick and Frazer, 1987); however, it was developed mainly for crustal investigations. Surface waves were included in the process by Kerry (1981) and Kennett and Clarke (1983). The method was applied in limited cases in the field of reflection prospecting by Fertig and Müller (1978) and Temme and Müller (1982). Major obstacles for the routine use of this process include: complexity of the associated numerical computation of the integral equation, lack of established procedures for the selection of the proper values of the required parameters, and lengthier computation times.

The present study illustrates that certain rules and guidelines can be used to control the choice of these necessary parameters. By using the specific Earth model, computation becomes simple and more efficient. More importantly, clean synthetic seismograms can be generated without requiring costly experimental computer runs.

The Earth model can consist of any number of horizontal layers which overlie a half-space. Anelastic effects are included through the use of complex wave velocities (Ganley, 1981). The vertical-displacement spectrum of the model is computed by numerical integration. The synthetic seismogram is obtained by convolving the frequency response by the source spectrum and a consequent inverse Fourier transform (Temme and Müller, 1982).

ANALYTICAL RELATIONSHIPS

The expression for the vertical-displacement spectrum of a layered Earth, assuming acoustic waves only, is given by Temme and Müller (1982) as follows:

$$U_{zi} = -F(\omega)\,\omega^2 \int_0^\infty dp\, \frac{pq_i}{q_1} J_0(p\omega r) \times \left\{ A_i e^{-j\omega q_i (z - z_i)} - B_i e^{j\omega q_i (z - z_i)} \right\}, \qquad (1)$$

where U_{zi} = vertical displacement in layer i,
$F(\omega)$ = spectrum of the excitation function,
ω = angular frequency,
p = horizontal slowness,
$l_i = \omega q_i$; $q_i = [\alpha_i^{-2} - p^2]^{1/2}$ = vertical slowness,
α_i = *P*-wave velocity

$$= \alpha_i(\omega) = \alpha_r \left(1 + \frac{1}{\pi Q} \ln \frac{\omega}{\omega_r} + \frac{j}{2Q} \right),$$

ω_r = reference frequency,
Q = quality factor,
α_r = velocity (real) at reference frequency,
r = source-receiver separation,
J_0 = Bessel function of order zero,
A_i = amplitude of all upgoing waves in layer i,

Manuscript received by the Editor July 23, 1987; revised manuscript received July 25, 1988.
[1]Department of Geological Sciences, University of Saskatchewan, Saskatoon, Saskatchewan S7N 0W0
This investigation was supported by research and operating grants provided by the Geological Survey of Canada and the Natural Sciences and Engineering Research Council of Canada. We are grateful to Drs. Müller and Temme for the use of their original computer program.

B_i = amplitude of all downgoing waves in layer i,
z = depth of the receiver,
z_i = depth to the top of layer i; $z_1 = 0$,
$j = \sqrt{-1}$.

This equation is simplified if the receivers are placed on the surface, as is the case in the present study. Putting $i = 1$ and $z = z_1 = 0$, we get:

$$U_{zi} = -F(\omega)\omega^2 \int_0^\infty pJ_0(p\omega r)[A_1 - B_1]\,dp. \tag{2}$$

A_1 and B_1 can be obtained from:

$$A_1 = -\left(RA_s + \frac{1}{A_s}\right)/(1+R), \quad B_1 = -A_1, \tag{3}$$

where R is the plane-wave reflectivity and $A_s = \exp(j\omega q_1 Z_s)$, Z_s being the depth of the source. R can be computed recursively using the relations:

$$R_{i-1} = \frac{r_i + R_i \exp(-j\omega q_{i-1} d_{i-1})}{1 + r_i R_i} \tag{4}$$

and

$$r_i = \frac{\rho_i l_{i-1} - \rho_{i-1} l_i}{\rho_i l_{i-1} + \rho_{i-1} l_i}, \tag{5}$$

where d_{i-1} is the thickness of $(i-1)$th layer and ρ_i is the density of the ith layer. The recursion is started with $i = n$, $R_n = 0$ and stopped at $i = 2$; the resulting R_1 is the reflectivity R. It should be further noted that the source is located in the first layer only.

Numerical computation of U_{zi}

The integral to be evaluated numerically is

$$-2\int_0^\infty pJ_0(p\omega r)\frac{\left(\frac{1}{A_s} + RA_s\right)dp}{(1+R)}. \tag{6}$$

The discrete form for computation of U_{zi} is

$$U_{zi} = \sum_{k=2}^{K} J_0\{(k-1)\Delta p\left(\omega - \frac{j}{\tau}\right)r\}\{(k-1)\Delta p\}\Delta p\left(\frac{1}{A_s} + RA_s\right)/(1+R), \tag{7}$$

where $K = (p_{max}/\Delta p) + 1$; p_{max} being the upper limit of p used in the summation. Δp is the slowness summation interval and τ is a damping factor introduced to suppress time-domain aliasing.

Parameter Selection

To obtain the synthetic seismograms using the previous equations, one must first establish the following:

(a) Earth model — this includes the P-wave velocity, density, thickness and Q of the different layers.
(b) Survey parameters — these comprise depth of source and source-receiver separations.
(c) Slowness — this requires selection of the maximum value of p and the interval Δp. Also, in certain instances it is useful to apply a cosine taper from some value of p less than p_{max} up to p_{max}, in which case the former also has to be selected.
(d) Damping factor — this is a function of the record length.
(e) Frequency — that is, the minimum and maximum values of ω.
(f) Kernel function — for the numerical evaluation of the Bessel function the computational procedure allows the use of either a polynomial approximation or the equivalent Hankel approximation.
(g) Source function — this is selected according to the expected survey source characteristics.

For a given earth model, the clarity of the derived theoretical response is dependent on the accuracy of the preceding choices.

The significance of the foregoing remarks is illustrated by two examples. The pertinent numerical data for these models are presented in Table 1.

MODEL 1

THICK.	VELOCITY	DENSITY	ATTENUATION
90m	Vp = 2975 $\frac{m}{s}$	= 2200 $\frac{kg}{m^3}$	Q = 100
527m	Vp = 4420	= 2500	Q = 200
131m	Vp = 4200	= 2400	Q = 200
267m	Vp = 5250	= 2650	Q = 300
402m	Vp = 5800	= 2700	Q = 350
374m	Vp = 6150	= 2800	Q = 400
	Vp = 6590	= 2900	Q = 500

Total no. of receivers : 24

Maximum source-receiver separation : 690m

MODEL 2

900m	Vp = 3000 $\frac{m}{s}$	= 2300	Q = 150
10m	Vp = 6000	= 2700	Q = 400
350m	Vp = 3500	= 2450	Q = 250
	Vp = 4500	= 2500	

Total no. of receivers : 24

Maximum source-receiver separation : 690m

Table 1. Layer parameters for Models 1 and 2.

Slowness p_{max}

The setting of an upper limit, p_{max} , on the slowness, p, in the numerical evaluation of equation (7) leads to a truncation phase in the computed seismograms (Aki and Richards, 1980). A commonly used value for p_{max} is $1/\alpha_1$, where α_1 is the P-wave velocity of the topmost layer. This choice of p_{max} gives rise to a truncation phase which virtually coincides with the direct wave. The latter is, therefore, distorted. Such a distortion may be acceptable if the arrivals of interest are at times later than the times of direct arrivals. For near-surface interfaces, the presence of these distorted phases may cause undesirable interference. Furthermore, if the arrivals of the head wave and the direct wave are close enough, a complex phase will result.

Figure 1 shows the features discussed above in the case of Model 1. The arrows labelled R_1, M_1. . . R_3 mark the two-way times for the first three interfaces and the three multiples. The source depth in this case is 1 m and p_{max} = 1/2975 s/m. The dominant truncation phase interferes with and masks the earliest reflection event, R_1, while the other events remain essentially undisturbed. Choosing $p_{max} = (V_{surface})^{-1}$ will place a set of strong truncation events along a linear pattern established by the direct traveltime of this apparent wave trend. Therefore, p_{max} should not be chosen according to the above criterion.

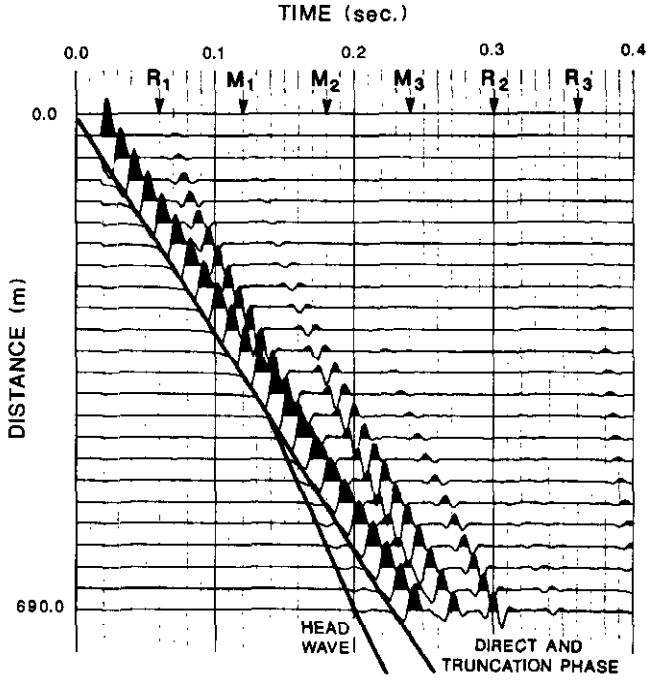

Fig. 1. Display of the first 0.4 s of the1-s record generated for Model 1. It shows the masking of the earliest reflection event, R_1, by the direct and truncation phases caused by a very shallow source (depth = 1 m) and without the application of a cosine taper on slowness p. First-break energy is overemphasized on the outside traces because of artificial enhancements of the truncation phase. Dominant source frequency is 50 Hz; damping factor τ = 1 s.

A simple way (if acceptable, given the problem at hand) to suppress the truncation phase substantially is to increase the source depth. Figure 2 illustrates this reduction by increasing the source depth to 10 m. The event R_1 can now be traced through a large number of traces.

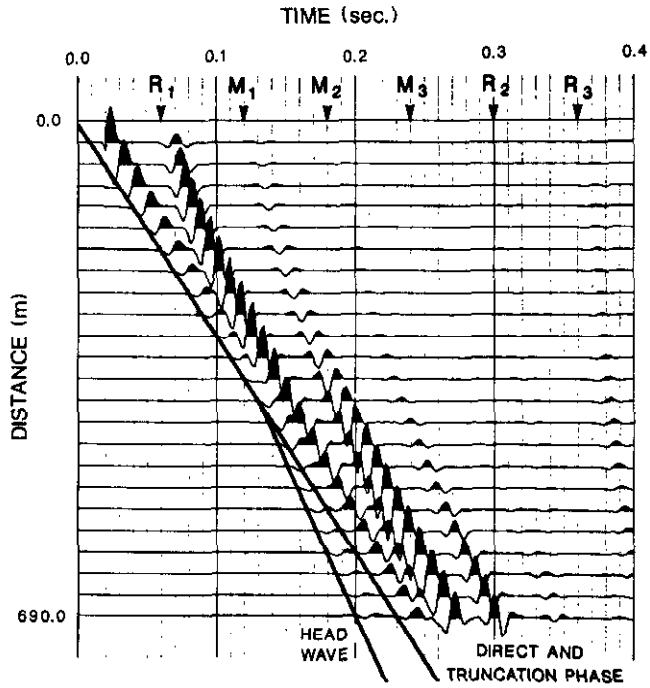

Fig. 2. Enhancement of the reflection event R_1 for Model 1 caused by increased source (depth = 10 m); no cosine taper applied on slowness, p. Dominant source frequency is 50 Hz; damping factor τ = 1 s.

If the source depth must remain shallow, then two procedures may be used to obtain suitable synthetics. In the first instance, the upper limit of p is set at $T/\Delta x$, where T is the largest arrival time of interest and Δx is the smallest source-receiver separation. The consequence of this choice is that the truncation phase is placed beyond the time zone of investigation. Unfortunately, this approach generally leads to a lengthy increase in the computation time that results from the large increase in the parameter K in the summation involved in equation (7).

The other procedure utilizes the effect of a cosine taper applied from a value of p less than p_{max} to p_{max} itself. Both p and p_{max} have to be chosen. Recognizing that the application of a cosine taper on slowness is akin to a velocity (or slowness) filter, the choice of p and p_{max} must ensure that no valid event is affected or, in an extreme case, filtered out completely. Thus in the case at hand, p was set at $1/\alpha_1$ (= 1/2975 s/m) and p_{max} at 1/675 s/m. The first value ensures the presence of the direct wave (Figure 3). The latter value is essentially arbitrary; it was chosen so that the truncation phase corresponding to it (if no cosine taper were applied) for the last trace would arrive at about 1.024 s — the computed length of the record. As is evident from Figure 3 the truncation phase resulting from the use of the cosine taper has been reduced to such an extent that the event R_1 can be traced throughout the seismogram. In view of the much lower computation time needed here, we recommend this approach over the previous one.

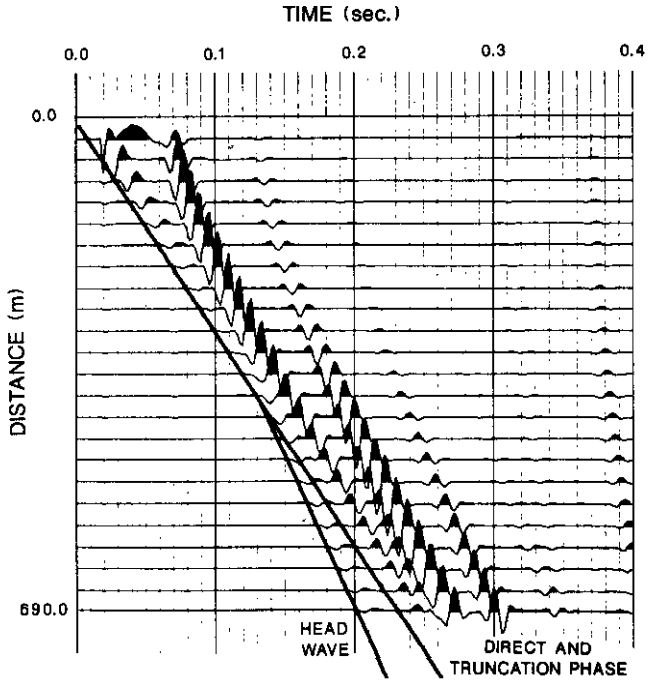

Fig. 3. Enhancement of the reflection event R_1 for Model 1 due to the application of a cosine taper on slowness p from p = 1/2975 s/m to p_{max} = 1/675 s/m. Dominant source frequency is 50 Hz; damping factor τ = 1 s.

Integration interval Δp

The selection of the integration interval, Δp, critically influences the overall signal-to-noise ratio level of the synthetic seismogram. This is especially so when the reflection coefficients are low or where the reflections from the deep horizons are computed with small source-receiver separations.

Once the earth model and the source-receiver separations are established, there are two simple ways in which the magnitude of Δp can be estimated. The first is based on the raypath equation of a two-layer earth model. The traveltime, T_r, is given by:

$$T_r^2 = T_0^2 + \frac{r^2}{V_1^2}. \tag{8}$$

T_0 is the zero-offset arrival time and r is the source-detector separation. The slowness associated with the ray is

$$p = \frac{dT_r}{dr} = \frac{r}{T_r V_1^2}. \tag{9}$$

Substituting for T_r from (8), the gradient is

$$\frac{dp}{dr} = \frac{1}{V_1^2 T_0 \left[1 + r^2/\left(T_0^2 V_1^2\right)\right]^{3/2}}. \tag{10}$$

It is proposed that Δp be given by:

$$\Delta p = \frac{dp}{dr}\Delta r, \tag{11}$$

where Δr is the receiver interval.

In the normal exploration surveying process, the spacing between detectors is uniform; therefore equation (11) can be rewritten as:

$$\Delta p = \frac{1}{V_1^2 T_0 (\Delta r)^2 \left[\frac{1}{(\Delta r)^2} + \frac{n^2}{T_0^2 V_1^2}\right]^{3/2}}, \tag{12}$$

where $r = n\Delta r$ at the nth detector location. This requires a different value of Δp for each receiver location. For simplification, one can use a single value of Δp calculated for the last receiver. Since Δp decreases as n increases and since a lower value of Δp will always ensure higher signal-to-noise ratio, the value of Δp so determined will be appropriate for all receivers. This is the procedure used in this study.

In the case of a multilayered earth, V_1 in equation (12) should be replaced by V_{rms} where

$$V_{rms} = \left[\frac{1}{T_0}\sum_{j=1}^{J}\left(V_j^2 \Delta T_j\right)\right]^{1/2}. \tag{13}$$

V_j is the interval velocity in the jth layer, ΔT_j is the two-way traveltime in the same layer and T_0 is the two-way traveltime at zero offset. It must be emphasized that equation (12) does not contain frequency considerations. Therefore, it provides only a starting approximation for Δp. Computations using this Δp value will lead to well defined events if they originate at shallow depths, but deeper reflections may be obscured by noise (Figure 4, beyond 0.5 s).

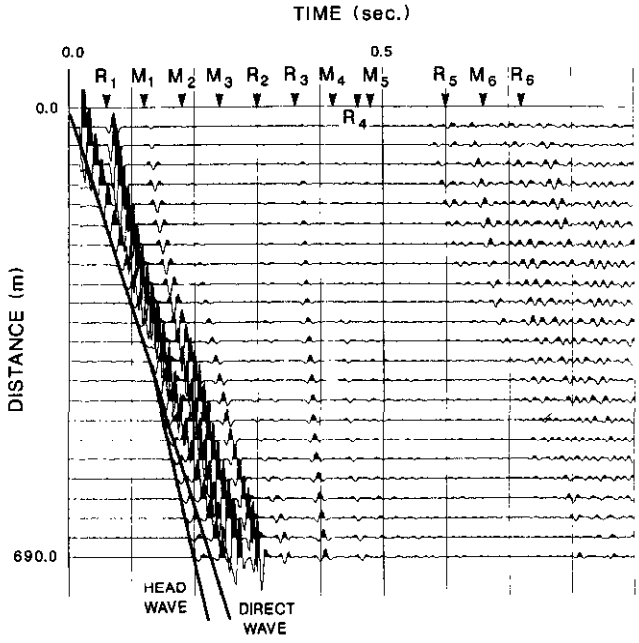

Fig. 4. Synthetic seismogram for Model 1; source depth is 10 m. Dominant source frequency is 50 Hz; damping factor τ = 1 s. There is no cosine taper on slowness p; there are, however, cosine tapers on the source spectrum from 30 Hz to 1 Hz and from 130 Hz to 150 Hz. Interval $\Delta p = 1.56 \times 10^{-6}$ s/m based on equation (12), which yields K = 217 in equation (7).

Another estimate of Δp can be arrived at by considering the characteristic behavior of the Bessel function J_0 ($p\omega r$). This is an oscillating function (Båth and Berkhout, 1984) whose peak amplitude decoys with increasing $p\omega r$. The first zero of J_0 ($p\omega r$) occurs at $p\omega r = 2.405$. This range of $p\omega r$, from 0 to 2.405, is here referred to as the first quadrant. By assigning a criterion of:

$$\omega_{max} r_{max} \Delta p = 1 , \tag{14}$$

where r_{max} is the maximum source-receiver separation, values of $p\omega r$ within the first quadrant are ensured for at least two samples if the numerical integration is computed for the maximum frequency and the most distant receiver. The value of Δp determined by equation (14) will yield at least two samples within the first quadrant for all the lower frequencies and shorter receiver separations. If the maximum frequency is chosen at the Nyquist level, which in turn is generally significantly higher than the dominant source frequencies, then a sufficiently close sampling of the Bessel function is secured.

Generally, the value of Δp determined from equation (14) is lower than the value provided by equation (12). The selection of the lower value of Δp ensures better defined, noiseless synthetics. It can also increase computational costs considerably. Use of very fine summation intervals becomes especially important when response characteristics of deeper reflectors are studied with associated small reflection-coefficient contrasts and near source-receiver configurations. According to Frazer and Gettrust (1984), Filon's method for the quadrature of oscillatory integrals does not require as refined a selection of Δp as the normal quadrature techniques in order to evaluate the reflectivity integral numerically. The efficiency of this computation process appears only in those cases where the source and receiver are many wavelengths apart or when the depth to the reflectivity zone is much greater than its thickness. These conditions are rather restrictive in exploration environments.

Figures 4 and 5 show the synthetics computed for Model 1 using the values of Δp calculated from equations (12) and (14). The two values were 1.56×10^{-6} and 9.23×10^{-7}, respectively. The two-way times for the reflected and multiple events corresponding to the respective interfaces are shown by R_1, M_1, etc. Three points need to be emphasized here. First, the Δp values calculated using the two criteria do indeed yield correct synthetics. Second, as mentioned above, the use of the finer summation interval (Figure 5) eliminates the noise which obscured the deeper reflection events R_5 and R_6 in Figure 4. Third, automatic gain control has been applied to all the traces shown. If a still smaller value of Δp is used, some of the noise seen towards the end of the records in Figure 5 can be eliminated. This is confirmed in Figure 6a which was computed using a value of $\Delta p = 4.61 \times 10^{-7}$, that is, half of the value used for Figure 5.

The very weak events marked H (Figure 6a), which arrive at an apparently infinite velocity, are due to the use

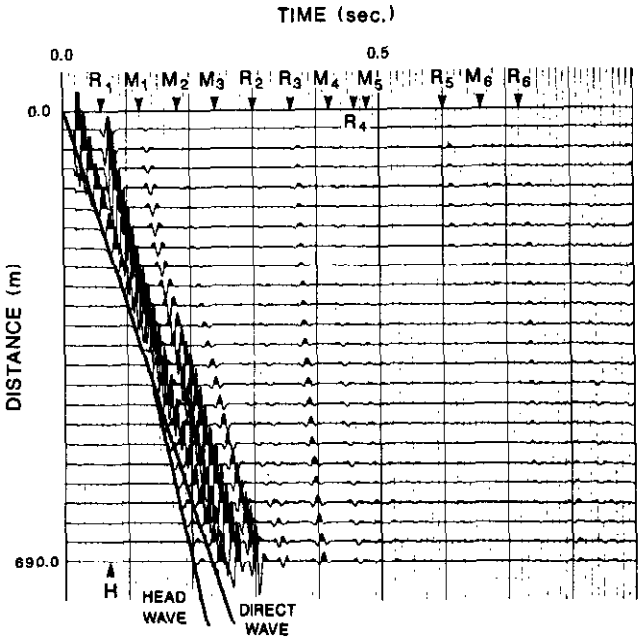

Fig. 5. Synthetic seismogram for Model 1. Interval $\Delta p = 9.23 \times 10^{-7}$ s/m based on equation (14) which yields $K = 365$ in equation (7). Other data are equivalent to those used in Figure 4.

of the Hankel approximation of the Bessel function during the computation. The small kinks in the inner traces at 0.02 s are due to numerical noise also related primarily to this cause. These features will be discussed later.

The weak reflected or multiple events, especially beyond 0.5 s in Figure 6a, are displayed very clearly in Figure 6b. This enhancement of the amplitudes was achieved by computing the synthetics with parameters identical to those used to obtain Figure 6a, but with one difference. The amplitudes of the traces in Figure 6b were scaled by an exponential function of time, namely, $\exp(6t)$.

The CPU times on a VAX 11/785 taken to compute the complete synthetics (that is, 24 traces with 512 points each) shown in Figures 4 to 6 were about 11, 21 and 42 minutes, respectively. As expected, the times relate directly to the integration interval Δp, other parameters remaining unchanged. Clearly, for a given record length, the computation time will increase if one or more of the following parameters are increased: number of layers, frequency range of computation, and number of traces.

Damping factor τ

The desired time length of the synthetic response $u(t)$ is T_D ($0 < t < T_D$), which, in the present application, is the two-way traveltime of the reflected energy from the top of the half-space. A complicated earth model normally generates recognizable responses in time T_f beyond the desired time window ($T_f >> T_D$). If the computational time window, T_c, is chosen to be shorter than T_f, the neglected events will not be suppressed but will appear in the early part of the time-domain seismograms as wrapped-around events.

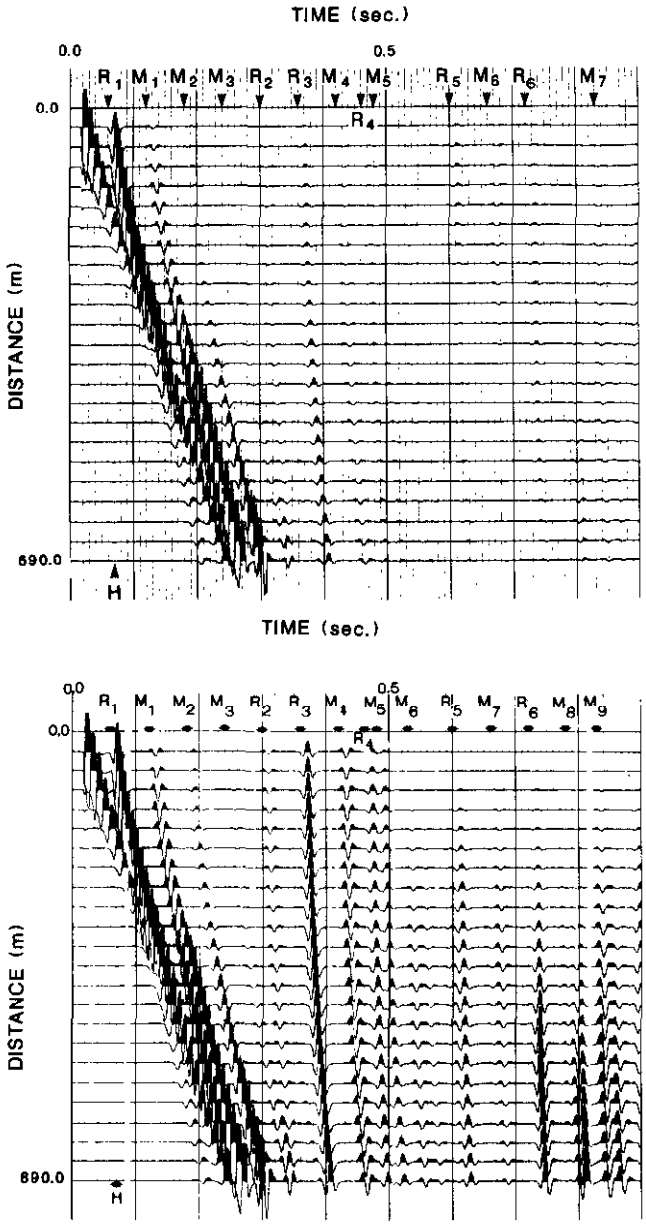

Fig. 6. **(a)** Synthetic seisomogram for Model 1. Interval $\Delta p = 4.61 \times 10^{-7}$ s/m which yields $K = 730$ in equation (7). Other data are as used in Figure 4.
(b) Synthetic seismogram for Model 1. All parameters used for computation are the same as in Figure 6a. The amplitude of the later events are enhanced due to the use of an exponential scaling function of time [exp (6t)]. The number of multiple events marked here exceeds that of Figure 6a.

Theoretically, the response time of an earth model is infinitely long. In practice, the amplitudes of these late events are attenuated down to the noise level at a final time beyond the reflection time for the deepest reflector. Ganley (1981), as a rule of thumb, proposed that T_c should be four to eight times T_D. This empirical approach leads to solutions at a high computational cost. Temme and Müller (1982) attempted to eliminate the aliasing effects by computing damped seismograms. They developed a damping factor by implementing conditions established by Bouchon (1979). A highly damped seismogram is obtained by computing $U_\tau(t) = u(t)e^{-t/\tau}$ instead of $u(t)$, which represents convolutions at complex frequencies $\left(\omega - \frac{j}{\tau}\right)$ rather than ω. The desired seismogram, $u(t)$, is then obtained by multiplying $U_\tau(t)$ in the desired time window with $e^{t/\tau}$. The condition imposed by Bouchon is that

$$u(t) >> u(t+T)e^{-t/\tau}, \tag{15}$$

where T is any time beyond T_D. The condition in (15) forces the level of all later responses to be smaller than the desired events but provides no analytic means for proper selection of the damping parameter τ.

Since the arrivals occurring later than T_D are multiples, a careful examination of the response function of the model will lead to the proper selection of τ. If one considers a realistic multilayered earth model and limits the calculation to vertically incident energy only, then every interface is associated with its reflection coefficient r_{lm} (for interface l, m) and a corresponding two-way traveltime. The behavior of these parameters with respect to the amplitudes of the relevant multiples is illustrated in Table 2, which was prepared by assuming that the source amplitude is unity.

	(Interface ℓ,m) TWO-WAY TIME	REFLECTED AMPLITUDE
Primary	$T_{\ell m}$	$r_{\ell m}$
1st multiple	$2T_{\ell m}$	$r^2_{\ell m}$
2nd multiple	$3T_{\ell m}$	$r^3_{\ell m}$
nth multiple	$(n+1)T_{\ell m}$	$r^{n+1}_{\ell m}$

Table 2. Two-way times and reflected amplitudes corresponding to different interfaces. Source amplitude is assumed equal to unity and incidence is vertical.

Under most realistic conditions $r_{lm} << 1$; therefore, although the amplitudes of the multiples naturally fulfill the conditions imposed by equation (15), these amplitudes still can exceed the noise level, N. If the arrival times of such multiples exceed T_D, they shall appear as wrapped-around events in the early part of the records. The aim, then, is to reduce the amplitude of these events to the noise level. Analytically, this means:

$$r_{lm}^2 \exp\left(-T_{lm}/\tau\right) = N \tag{16}$$

or,

$$\exp\left(-T_{lm}/\tau\right) = N/r_{lm}^2 . \tag{17}$$

By setting the noise level at an appropriate low value, τ can be determined. Because N/r^2_{lm} will be less than unity,

$$-\frac{T_{lm}}{\tau} = \ln\left(\frac{N}{r^2_{lm}}\right) = -B\,, \tag{18}$$

that is:

$$\tau = \frac{T_{lm}}{B}\,. \tag{19}$$

In a given example of a multilayered earth, multiple traveltimes $(n + 1)\,T_{lm} > T_D$ are the only multiples that have to be suppressed. Furthermore, r_{lm} will now refer to the largest reflection coefficient. If the noise level is set at $N = 0.001$ (– 60 dB) and a typical spectrum of reflection coefficients is considered, then τ generally lies between 20 and 60 percent of T_D. Similar values were suggested by Temme and Müller (1982) on empirical grounds.

Figures 7 and 8 illustrate the synthetics for Model 2 computed for two values of τ. For Figure 7, $\tau = 99.0$ was used, which, in effect, means that no damping was applied to multiple events beyond T_c (= 1.024 s). This results in two wrapped-around events A_1 and A_2. A_1 corresponds to the first multiple of R_1. Note here that A_1 occurs at $(2 \times 0.6 - 1.024)$ s = 0.176 s. A_2 can be either the third multiple of R_1 (corresponding to an arrival time of 2.4 s) or may be caused by a reflection path involving the first interface, the surface boundary and the second interface. An auxilliary computation showed that the second alternative is correct.

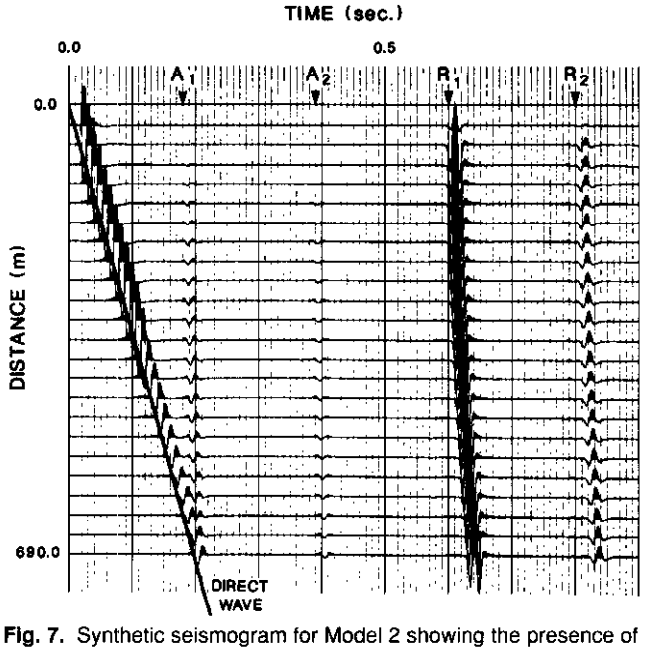

Fig. 7. Synthetic seismogram for Model 2 showing the presence of two wrapped-around 'multiple' events, A_1 and A_2. These events are present because the damping factor τ equals $99T_c$, where T_c (= 1.024 s) is the length of the record computed. R_1 and R_2 are the reflection events from the base of the first and the last layers, respectively. Computations were done using the polynomial approximation for the Bessel function J_0.

For Figure 8, the value of $\tau = 0.2T_D$ was determined as outlined in Table 2 and equation (19). The most striking

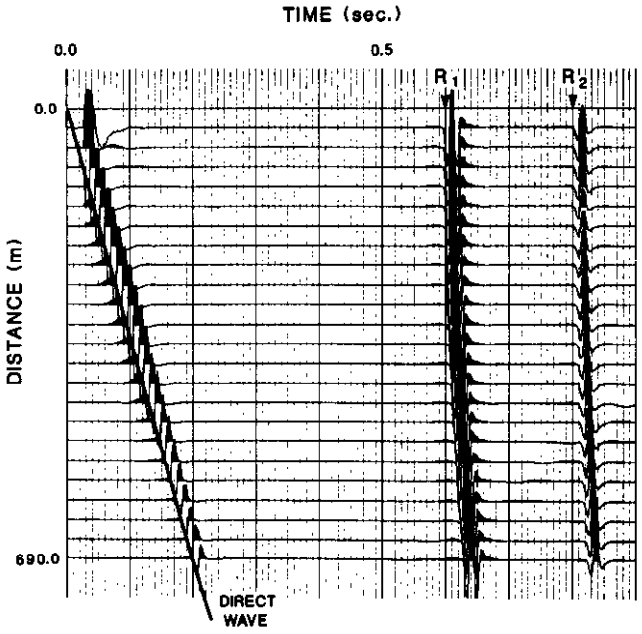

Fig. 8. Synthetic seismogram for Model 2 in which the two wrapped-around events, A_1 and A_2 (Figure 7), are absent, since the damping factor here equals $0.2T_c$.

change from Figure 7 is the elimination of the two wrapped-around events.

It may be mentioned here that the selection of the damping factor for the synthetics computed for Model 1 (Figures 1 to 6) was also based on considerations similar to those applied for Figure 8. In these cases, the value of τ chosen exceeded the limits suggested by Temme and Müller (1982). No wrapped-around events, however, are observed in any of the synthetics in Figures 1 to 6, supporting the need for our more general approach in the selection of the damping factor.

Choice of computational formula for the Bessel function

The computation of the vertical displacement spectrum involves the summation of the right-hand side of equation (7). The evaluation of the Bessel function $J_0(x)$, where the argument x is $(k - 1)\Delta p\left(\omega - \frac{j}{\tau}\right)r$, has been done using either the Hankel approximation or a pair of polynomial approximations given by Abramowitz and Stegun (1965). Either choice may lead to some undesirable features in the computed synthetics. Since J_0 is not truly periodic for small arguments, a reasonable choice is to use polynomial approximation for low arguments and asymptotic approximation at higher arguments. However, limited attempts using this approach with $x = 3$ as the switchover value still produced some noise in the innermost traces.

The Hankel approximation is given by $\left(\frac{1}{2\pi x}\right)^{1/2} \exp\left[-j\left(x - \frac{\pi}{4}\right)\right]$. This representation implies that only the diverging waves from the source are being considered, and thus it is meaningful in physical terms and

is the one most appropriate to use. A problem arises when $x \rightarrow 0$. For a receiver with zero offset ($r = 0$) and vertical incidence ($p = \Delta p = 0$), the approximation obviously is not valid. For small offsets (as in reflection seismology), the summation at a given frequency ω, and involving increments of Δp, will therefore be in error because of the erroneously high values associated with the Hankel approximation at the very small initial values of $(k-1)\Delta p$ ($\Delta p \approx 10^{-7}$). In other words, numerical noise is being introduced due to the Hankel approximation in the frequency-domain calculation for all frequencies of interest and for all receivers. After inverse Fourier transformation, this noise will appear in the time domain either as a general background noise or as unwanted events for every receiver. Since the noise is distributed over a range of frequencies, it will show up as a fictitious arrival on all traces. Furthermore, these events seem to have an almost infinite phase velocity "arriving" at times corresponding to the two-way times for the shallowest reflector. The amplitudes of these events are relatively very weak except in the case where the first interface has a large associated reflection coefficient. This explains the presence of the weak events marked H in Figures 4 to 6. Synthetics shown in Figures 7 and 8 were computed using the polynomial approximation instead of the Hankel. Numerical noise in the initial parts of the traces is almost absent (cf., that associated with the events H in Figures 4 to 6).

An interesting comparison can be made between Figure 7 and Figure 9. The latter was computed with the very same parameters as Figure 7 but using the Hankel approximation. Two features show up in Figure 9. One is the spike at 0.02 s, which is related to numerical noise, and the other is a small-amplitude precursor event H associated with the arrival R_1 on the outer traces. These events show very insignificant moveout; that is, they possess an almost infinite apparent velocity. They are an example of the unwanted events discussed earlier in this section, although the first interface in this case is certainly not shallow. The reason why the event H still appears is due to the very strong impedance contrast between the first two layers in Model 2.

The use of the polynomial approximation helps to reduce substantially the amplitude of the numerical noise and spurious events in the very early part of the traces. A problem with this approach, however, is the presence of truncation events towards the end of the traces *(I)* but in the incoming direction (e.g., Figure 10, which displays the seismogram for Model 1). Thus, the event occurs later in time as the distance to the source decreases. Its velocity corresponds to the inverse of the maximum value of slowness chosen for numerical integration. It should be noted that the use of the cosine taper on maximum slowness helps to remove the truncation event in the ingoing direction. The rest of the seismogram remains unchanged. Another way to avoid the presence of such events in the time zone of investigation is to compute a record length large enough that these events fall beyond the reflection times of interest.

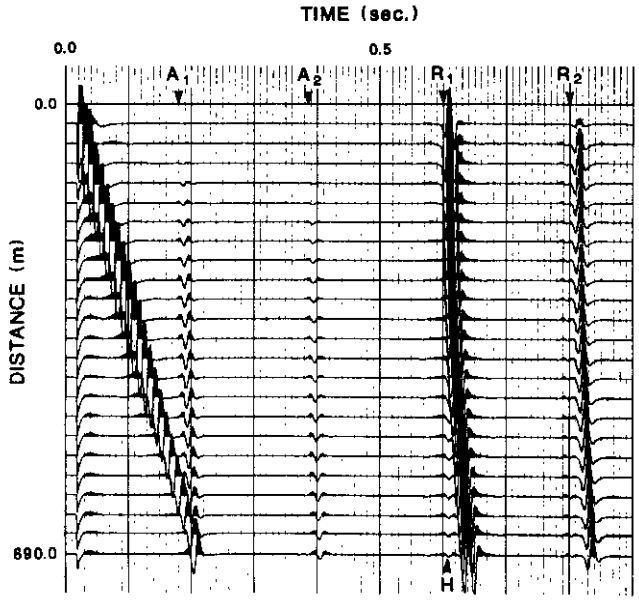

Fig. 9. Synthetic seismogram for Model 2 showing the effect of using the Hankel approximation for J_0. Other data are used in Figure 7. Computations yield two unwanted events: one at 0.02 s and the other a precursor to the event R_1.

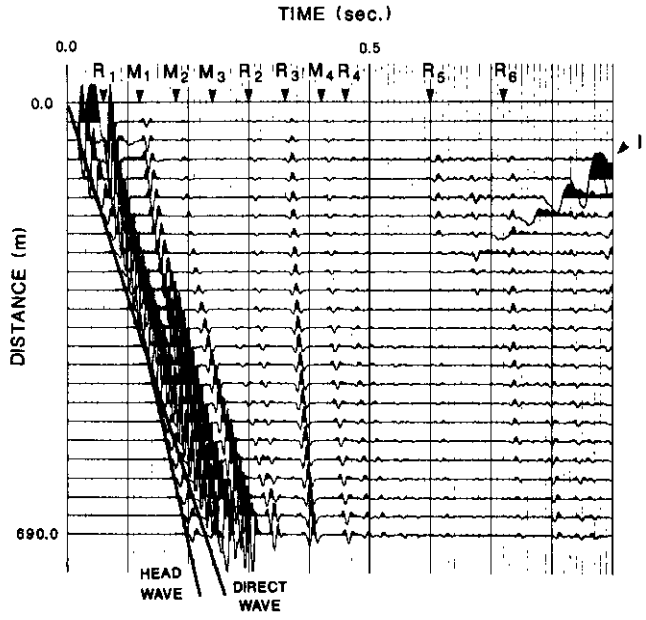

Fig. 10. Synthetic seismogram for Model 1 showing the presence of truncation events, *I*, due to the use of the polynomial approximation of the Bessel function.

Our experience with a variety of models leads us to conclude that in most cases of interest the use of the Hankel approximation will yield acceptable synthetics. These observations are in accordance with comments of Temme and Müller (1982).

Choice of frequencies

The theoretical minimum frequency used in the computation is set by the record length itself. In practice, the min-

imum frequency is a choice set by the instrument responses of the geophones used. The synthetics computed using the theoretical value (as in the case in the present study) will, if anything, contain more information than is recorded in the field. The maximum frequency obviously should be high enough to cover the entire source spectrum. In the present study, the source function used is given by:

$$f(t) = \sin\left(\frac{m\pi t}{T}\right) - \frac{m}{m+2}\sin\frac{(m+2)\pi t}{T} \quad (0 < t < T)$$
$$= 0 \quad (t < 0,\ t > T)$$

where

$m = 2$ and $T = 0.02$ s.

The dominant source frequency used was 50 Hz. Figure 11 shows the main source spectrum along with the minor side lobe. The lower and the higher frequency limits were 1 Hz and 150 Hz, respectively. The effect of applying cosine tapers to the two frequency limits is also shown in Figure 11. Tapers (a) and (c) produced the best synthetics. The main point to note is that the appropriate use of cosine tapers not only helps to establish a tight control on the source spectrum but also to produce clean synthetics.

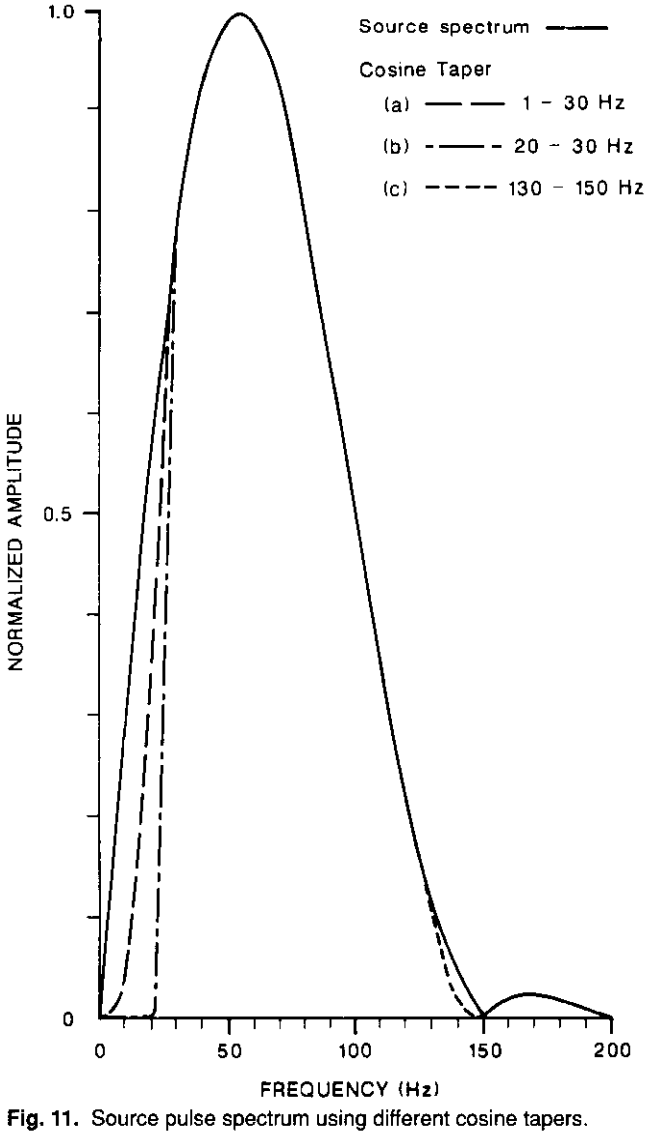

Fig. 11. Source pulse spectrum using different cosine tapers.

Conclusions

1. The reflectivity method permits efficient computation of a multitrace response of a complex earth model.
2. The proper selection of computational parameters provides an easy control over the development of the undesirable numerically generated artifacts. All expensive multicomputational experimental runs are eliminated.
3. The parameters are automatically derivable from the properties of the selected earth model.
4. Wisely chosen cosine tapers help, not just in the noise suppression but also in controlling the signal frequency characteristics of the different arrival sets, allowing modelling of intricate arrival-interference patterns.
5. The simultaneous computation of many spatially arranged traces allows the study of relationships among all forms of arrivals, including all possible multiples and converted events.

References

Abramowitz, M. and Stegun, I.A., 1965, Handbook of mathematical functions: Dover Publ. Inc.

Aki, K. and Richards, P.G., 1980, Quantitative seismology, Vol. 1: W.H. Freeman & Co.

Båth, M. and Berkhout, A.J., 1984, Mathematical aspects of seismology, 2nd Ed.: Geophysical Press.

Bouchon, M., 1979, Discrete wave number representation of elastic wave fields in three-space dimensions: J. Geophys. Res. **84**, 3609-3614.

Fertig, J. and Müller, G., 1978, Computations of synthetic seismograms for coal seams with the reflectivity method: Geophys. Prosp. **26**, 868-883.

Frazer, L.N. and Gettrust, J.F., 1984, On a generalization of Filon's method and the computation of oscillatory integrals of seismology: Geophys. J. Roy. Astr. Soc. **76**, 461-481.

Fryer, G.J., 1980, A slowness approach to the reflectivity method of seismogram synthesis: Geophys. J. Roy. Astr. Soc. **63**, 747-758.

Fuchs, K., 1968, The reflection of spherical waves from transition zones with arbitrary depth-dependent elastic moduli and density: J. Physics of the Earth **16**, 27-41.

_____ and Müller, G., 1971. Computation of synthetic seismograms with the reflectivity method and comparison with observations: Geophys. J. Roy. Astr. Soc. **23**, 417-433.

Ganley, D.C., 1981, A method for calculating synthetic seismograms which include the effects of absorption and dispersion: Geophysics **46**, 1100-1107.

Kennett, B.L.N., 1974, Reflections, rays, and reverberations: Bull. Seis. Soc. Am. **64**, 1685-1696.

_____ , 1979, Theoretical reflection seismograms for elastic media: Geophys. Prosp. **27**, 301-321.

_____ , 1980, Seismic waves in a stratified halfspace—II. Theoretical seismograms: Geophys. J. Roy. Astr. Soc. **61**, 1-10.

_____ , 1983, Seismic wave propagation in stratified media: Cambridge Univ. Press.

_____ and Clarke, T.J., 1983, Seismic waves in a stratified halfspace—IV: *P-SV* wave decoupling and surface wave dispersion: Geophys. J. Roy. Astr. Soc. **72**, 633-645.

Kerry, N.J., 1981, Synthesis of seismic surface waves: Geophys. J. Roy. Astr. Soc. **64**, 425-446.

Kind, R., 1978, The reflectivity method for a buried source: J. Geophys. **44**, 603-612.

_____ , 1979, Extensions of the reflectivity method: J. Geophys. **45**, 373-380.

Mallick, S. and Frazer, L.N., 1987, Practical aspects of reflectivity modeling: Geophysics **52**, 1355-1364.

Temme, P. and Müller, G., 1982, Numerical simulation of vertical seismic profiling: J. Geophys. **50**, 177-188.